Science Bulletin xxx (xxxx) xxx

Contents lists available at ScienceDirect

Science Bulletin

journal homepage: www.elsevier.com/locate/scib

Review

Adjustment methods of Schottky barrier height in one- and two-dimensional semiconductor devices

Jianping Meng [a,b,*], Chengkuo Lee [c,d,*], Zhou Li [a,b,*]

[a] Beijing Institute of Nanoenergy and Nanosystems, Chinese Academy of Sciences, Beijing 101400, China
[b] School of Nanoscience and Engineering, University of Chinese Academy of Sciences, Beijing 100049, China
[c] Department of Electrical and Computer Engineering, National University of Singapore, Singapore 117583, Singapore
[d] Center for Intelligent Sensors and MEMS, National University of Singapore, Singapore 117608, Singapore

ARTICLE INFO

Article history:
Received 1 November 2023
Received in revised form 10 January 2024
Accepted 2 February 2024
Available online xxxx

Keywords:
Schottky contact
Schottky barrier height
Adjustment methods
One- and two-dimensional semiconductor

ABSTRACT

The Schottky contact which is a crucial interface between semiconductors and metals is becoming increasingly significant in nano-semiconductor devices. A Schottky barrier, also known as the energy barrier, controls the depletion width and carrier transport across the metal–semiconductor interface. Controlling or adjusting Schottky barrier height (SBH) has always been a vital issue in the successful operation of any semiconductor device. This review provides a comprehensive overview of the static and dynamic adjustment methods of SBH, with a particular focus on the recent advancements in nano-semiconductor devices. These methods encompass the work function of the metals, interface gap states, surface modification, image-lowering effect, external electric field, light illumination, and piezotronic effect. We also discuss strategies to overcome the Fermi-level pinning effect caused by interface gap states, including van der Waals contact and 1D edge metal contact. Finally, this review concludes with future perspectives in this field.

1. Introduction

Metal-semiconductor contacts are a fundamental component of semiconductor devices. Among them, the Schottky contact is a vital type of metal–semiconductor contact, which arises due to (I) the disparity between the electron affinity of semiconductors and the work function of metals, as well as (II) the Fermi level pinning of the semiconductor [1–5]. The Schottky barrier is an energy barrier that can adjust the depletion width and carrier transport across the interface [6]. At a fixed bias voltage, the current and barrier height exhibit an exponential relationship, which makes the Schottky barrier crucial for the operation of any semiconductor device. Among them, devices constructed with nano-structured semiconductors, which exhibit unique physicochemical properties due to their physically confined structures in one dimension at least, have garnered significant attention. However, the intense scientific interest in SBH still pales in comparison with the pressure and demand to regulate SBH and solve the contact problem in nano-semiconductor devices. In the semiconductor industry, it is hoped to achieve zero SBH to reduce carrier injection barriers and contact. Conversely, a suitable SBH is necessary for the application of Schottky sensor. Therefore, adjusting the Schottky barrier height to obtain an appropriate value is crucial for electronic devices, as device performance can be significantly enhanced by adjusting the SBH [7,8].

This review summarizes the methods used to adjust the SBH in nano-semiconductor devices, including the work function of the metals, the interface gap states of nano-semiconductors, Fermi level pinning, surface modification, image-lowering effect, external electric field, light illumination, and piezotronic effect (Fig. 1), which is crucial to the research field and the semiconductor industry.

2. Condition and theory for the formation of Schottky barrier

In the ideal scenario, the SBH heavily depends on the work function of metal, as predicted by the Schottky-Mott theory [9,10]. According to this theory, the SBH of an n-type semiconductor is determined by the electron affinity of the semiconductor and the work function of the metal (Fig. 2a, Eq. (1)). For p-type semiconductors, the bandgaps of the semiconductors must be considered (Fig. 2b, Eq. (2)). However, in reality, the Schottky-Mott relationship (Eqs. (1) and (2)) does not align with experimental results. Specifically, the SBH is insensitive to the work functions metal

* Corresponding authors.
E-mail addresses: mengjianping@binn.cas.cn (J. Meng), elelc@nus.edu.sg (C. Lee), zli@binn.cas.cn (Z. Li).

https://doi.org/10.1016/j.scib.2024.03.003
2095-9273/

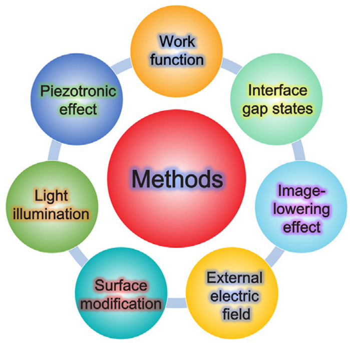

Fig. 1. (Color online) Adjustment methods of SBH.

owing to the Fermi level pinning. The Fermi level pinning effect caused by interface gap states, such as surface defects, chemical bonding, and surface dipoles [6,11,12], must be considered in the determination of Schottky barrier height. This effect is particularly pronounced in nanomaterials with a high surface-to-volume ratio [13].

$$q\phi_{\mathrm{Bn0}} = q\phi_{\mathrm{m}} - q\chi_{\mathrm{S}}, \tag{1}$$

$$q\phi_{\mathrm{Bp0}} = E_{\mathrm{g}} - q(\phi_{\mathrm{m}} - \chi_{\mathrm{S}}), \tag{2}$$

where $q\phi_{\mathrm{Bn0}}$ is SBH for the n-type semiconductor; $q\phi_{\mathrm{m}}$ is the work function of metal; $q\chi_{\mathrm{S}}$ is electron affinity of semiconductor; q is the unit electronic charge; E_{g} is the bandgap of semiconductor.

3. Adjustment methods of SBH

SBH dominates carrier transport across the metal–semiconductor interface. By adjusting the SBH, the detection performance of Schottky devices for gases, molecules, light, strain, and more can be enhanced [7].

3.1. Work function of metals

Despite the fact that SBH is insensitive to the work function of the metals, particularly in three-dimensional (3D) semiconductor materials, because the termination of three-dimensional semiconductor materials on the surface leads to strong Fermi level pinning, metals with high work function tend to form Schottky contacts with n-type semiconductors, while the results of p-type semiconductors are opposite. Additionally, low resistance metals can minimize their impact on the performance of Schottky device. Metals or metal-like materials with high work-function, such as Au, Ag, Pt, Pd, Cu, Ni, and graphene (metal-like), are typically preferred for forming Schottky contacts in n-type semiconductors [14]. The SBH is high when high work-function metals are selected. Fig. 3 summarizes the work functions of polycrystalline metals. The highest work function of Pt is 5.64 eV, and the lowest work function of cesium is 1.93 eV. Although the measured work functions of polycrystalline metals are constant, experimental data show that SBHs formed between polycrystalline metals and semiconductors are always inhomogeneous, as reflected in the *I*–*V* curve. This suggests that the work function varies with the exposed crystal planes. For instance, the work function of Pt ranges between 5.12 and 5.93 eV, depending on the crystal plane.

Unlike 3D materials, which have many surface dangling bonds, two-dimensional (2D) semiconductor materials have garnered renewed attention due to the absence of dangling bonds. These materials offer a promising approach to avoiding Fermi level pinning and chemical disorder, and they are expected to achieve a linear relationship with a slope of unity between SBH and the metal work function, which greatly facilitates the adjustment of Schottky barrier by changing metal work function. Pan et al. [15] attempted to adjust the SBH and carrier types of graphene by changing the contact metal. Ohmic or quasi-Ohmic contact is formed when graphdiyne contacts metals with low work functions, such as Al, Ag, and Cu. When graphdiyne contacts with Pd (SBH = 0.21 eV) and Au (SBH = 0.46 eV), an n-type Schottky barrier is formed. Higher work function metals such as Pt, Ni, and Ir, tend to form a p-type Schottky barrier with barrier heights of 0.30, 0.41, and 0.46 eV, respectively (Fig. 3b).

In the case of n-type few-layer MoS_2, a detailed temperature-dependent study reveals that SBHs are ~230, ~150, ~50, and ~30 meV for Pt, Ni, Ti, and Sc, respectively (Fig. 3c) [16]. The SBH increases with the increase of work function. The slope, or interface behavior parameter S ($S = \Phi_{\mathrm{SB}}/\Phi_{\mathrm{m}}$), is roughly 0.1, indicating the strong Fermi level pinning near the conductive band. Despite the work function of metal being pinned around the MoS_2 conduction band edge due to the Fermi pinning level effect, high work-function metals yield a high SBH [16]. To overcome the Fermi level pinning effect, an effective method, 1D edge contact, is proposed. Fig. 3d illustrates a clear distinction between the work function alignment for 1D edge contact and 2D surface contact [17]. Furthermore, a suitable metal can change the injection carrier (holes or electrons) type of field-effect transistors (FETs). It is found in the FETs of a single-wall carbon nanotube (CNT). The ballistic p-type CNT FETs are yielded when a single-wall CNT contacts with Pd (5.1 eV) [18–20], while ballistic n-type CNT FETs are produced when a single wall CNT contacts with Sc (3.3 eV) with a low work function (Fig. 3e) [21,22].

3.2. Interface gap states in semiconductors

Due to the surface termination of the finite crystal in a 3D periodic structure, surface states within the bandgap of semiconductors are created. This leads to surface dangling bonds, incomplete covalent bonds, or surface reconstructions, resulting in Fermi level pinning at these energy levels [23]. When metal and 3D semiconductor come into contact, a metastable structure interface is

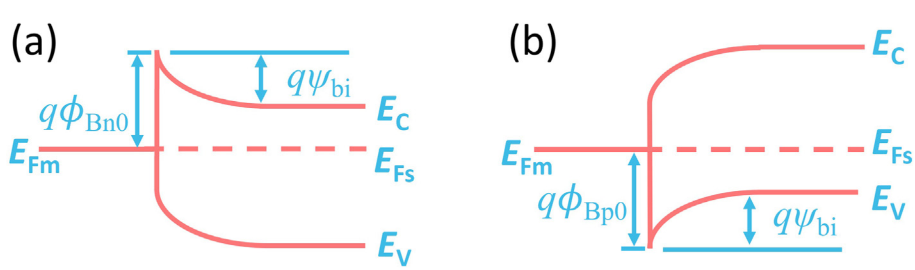

Fig. 2. (Color online) Energy band diagram of Schottky contact at metal–semiconductor interface. (a) n-type semiconductor, (b) p-type semiconductor. $q\phi_{\mathrm{B}}$ is SBH, ψ_{bi} is built-in potential.

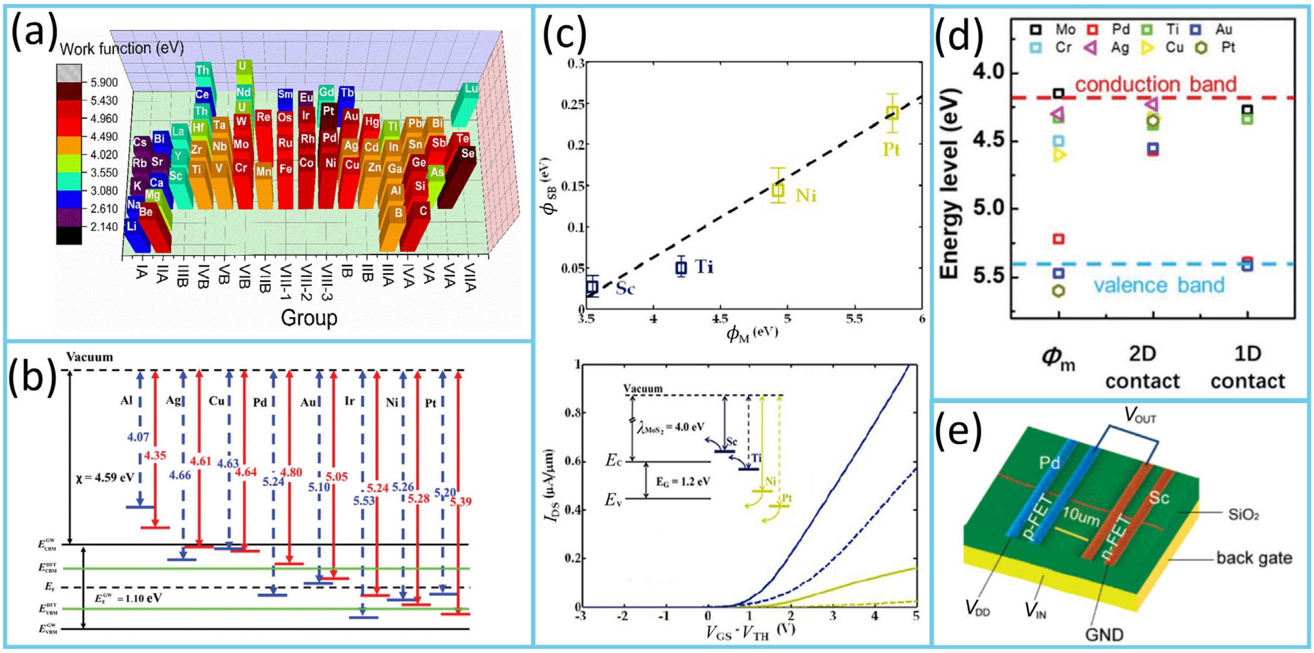

Fig. 3. (Color online) The influence of work function of metal on SBH. (a) Work function ϕ_m^{exp}(eV) of element in periodic table. Data obtained from polycrystalline specimens in Ref. [14]. (b) Line-up of work function of metal before and after contact with graphdiyne. Reproduced with permission from Ref. [15]. Copyright © 2009, Royal Society of Chemistry. (c) SBH of MoS_2 contacted with of Sc, Ti, Ni, and Pt, and its performance of transistor. Reproduced with permission from Ref. [16]. Copyright © 2013, American Chemical Society. (d) Work function alignment of metal-MoS_2 FETs. Reproduced with permission from Ref. [17]. Copyright © 2019, Wiley-VCH. (e) A single-walled CNT inverter composed of Pd CNT FET (p-type) and Sc-CNT FET (n-type). Reproduced with permission from Ref. [21]. Copyright © 2007, American Chemical Society.

formed, where unique electronic and atomic structures are formed to minimize energy. The presence of interface gap states can sustain local minima of free energy rather than global minima. Additionally, chemical bonding and interdiffusion at the metal–semiconductor interface can induce significant strain in both crystal lattices, change the band structures and lead to barrier [11,24,25]. The typical techniques for material fabrication and device integration often introduce an additional interface-trap state, serving as a reservoir for electrons or holes and causing Fermi level pinning [26]. The phenomenon of Fermi level pinning is closely related to the interface gap states in semiconductors (n-type in Fig. 4a and p-type in Fig. 4c).

Much causation about the formation of interface gap states has been proposed to explain the Fermi level pinning effect. They include surface states, metal-induced gap states (MIGS) [16], defect-related states, and disorder-induced gap states (DIGS) (Fig. 4b) [6,11,12]. The associated theories, including fixed separation theory, variable electron affinity theory, and bond polarization theory, have been proposed to quantify the impact of interface gap states on the Fermi level pinning effect [27].

The rise of 2D semiconductor materials brings us the opportunity to achieve an almost perfect surface without surface reconstructions, surface states, and surface dangling bonds. However, the defects always exist to maintain energy minimization due to an increase in entropy. Fermi level pinning in 2D semiconductor materials is associated with vacancy defects [28,29]. Therefore, it is crucial to prepare high-quality materials and minimize defects as much as possible to prevent Fermi level pinning. Moreover, during device preparation, defects such as atomic diffusion, strain, and point defects may be generated, especially if the metal electrode is prepared by deposition methods. The deposition process may generate defects, such as atom diffusion, strain, and point defects [30], and form chemical bonds at the interface, causing metal-induced gap states and interface dipoles [31–34]. Previous results indicate a strong Fermi level pinning at the metal–semiconductor interface, with pinning factors S of 0.11 and 0.07 for FETs based on monolayer MoS_2 and $MoTe_2$, respectively, after contact with the various deposited metals [35]. Kim et al. [35] introduced the charge neutrality level (CNL), which is defined as the energy above which the states of a neutral surface are empty, to quantify the Fermi level pinning. The CNL of MoS_2 and $MoTe_2$ is 4.48 and 4.77 eV, respectively (Fig. 5a). The Fermi level of MoS_2 is pinned around CNL near the conduction band, resulting in n-type conductivity in FETs. The Fermi level of $MoTe_2$ is pinned near the valence band, indicating that $MoTe_2$ FET has p-type conductivity.

A promising strategy to eliminate the Fermi level pinning effect from deposited metal is to insert an insulating layer or graphene [36–40]. Inserting an insulating layer creates a tunneling barrier, which reduces the charge injection efficiency. Moreover, due to its insulating nature, the band alignment of the insulator–metal contact cannot be tuned by the electric field. Introducing a thin *h*-BN film between the metal and MoS_2 can overcome Fermi level pinning and gate-dependent Schottky barriers (Fig. 5b), resulting in relatively free-moving conduction and valence bands [37]. Graphene, due to its strong tunability, serves as another viable buffer layer [41]. Using graphene as a buffer layer in the metal-$MoTe_2$/WSe_2 structure, a quasi-van der Waals contact is formed, significantly reducing the SBH and activation energies of thermionic emission, leading to excellent photoresponse performance (Fig. 5c) [40].

Van der Waals structures allow metal–semiconductor contacts without chemical bond formation, creating an almost perfect interface free from Fermi level pinning and chemical disorder [42–44], creating an approaching perfect interface free from Fermi level pinning and chemical disorder [30,42]. This allows the SBH in van der Waals structures to approach the Schottky-Mott limit, making SBHs highly adjustable and determined by the work function of metal (Fig. 5d). Despite the elimination of Fermi level pinning in top electrodes formed by van der Waals contact, the PMMA substrate can cause serious surface scattering of carriers. The

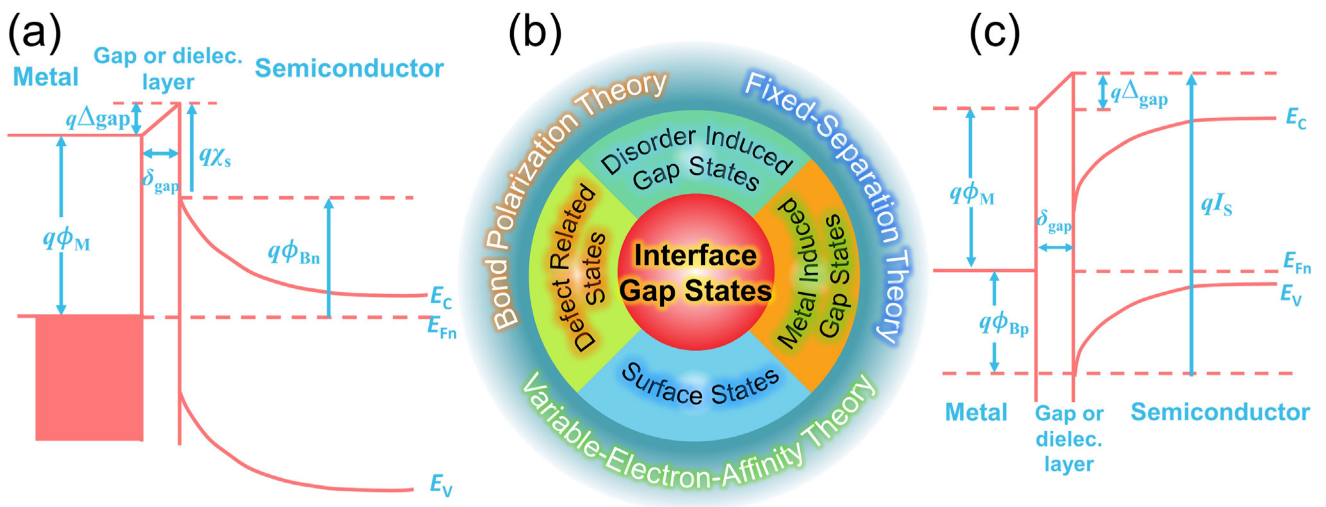

Fig. 4. (Color online) Interface gap states and corresponding theories. (a) A schematic of interface gap state model based on metal and n-type semiconductor interface. (b) The various sources and the theories of interface gap states. (c) A schematic of interface gap state model based on metal and p-type semiconductor interface. $q\phi_m$ is the work function of metal. $q\phi_{Bn}$ and $q\phi_{Bp}$ is Schottky barrier of n-type semiconductor and p-type semiconductor, respectively. δ_{gap} is the thickness of gap. Δ_{gap} is the potential drop in interface gap. $q\chi_s$ is the electron affinity of semiconductor. qI_s is the ionization energy of semiconductor.

inevitable gap between metal and 2D semiconductors might result in a tunnel barrier, lowering the charge injection efficiency. However, this tunnel barrier can be eliminated by choosing an appropriate metal. For instance, the tunnel barrier height is high when indium (In) is chosen as the contact metal for MoS_2 [45], but it is eliminated when Ti or Mo is used as the contact electrode [46]. Wang et al. [47] explored the creation of van der Waals contacts with low contact resistance in 3D metals and 2D semiconductors by electron beam evaporation at low temperatures and deposition rates. They successfully established ultraclean van der Waals contacts between a 10-nanometer-thick indium layer, topped with 100-nanometer-thick gold electrodes, and a monolayer of MoS_2. The interface was atomically sharp, with no observable chemical interaction, indicating the formation of van der Waals bond. Then, they further employ intermittent electron beam evaporation to maintain low temperatures and achieve high-performance p-type devices [48]. These devices approach ideal van der Waals interfaces without chemical interaction between Pd, Pt, and a few layers of MoS_2 and WS_2. The obtained p-type FETs with van der Waals contacts displayed several advantageous characteristics, including a low contact resistance of 3.3 kΩ μm, high mobility value of approximately 190 $cm^2\ V^{-1}\ s^{-1}$ at room temperature, saturation currents exceeding 10^5 A m^{-1}, and on/off ratio of 10^7. Kwon et al. [49] demonstrated the possibility to create interaction- and defect-free van der Waals contacts between various metals and 2D semiconductors by a metal deposition process with an expendable selenium buffer layer. The p-type WSe_2 field-effect transistors using gold van der Waals contacts show stable performance. While the performance is not superior to existing literature, this technique holds promise for mass device fabrication. Recently, Shen et al. [50] delved into the zero SBH between semi-metallic bismuth and semiconducting monolayer transition metal dichalcogenides (TMDs), and achieve ultralow contact resistance of 123 Ohm micrometers by sufficiently suppressing MIGS and spontaneously forming degenerate states. Despite numerous attempts in van der Waals contacted devices, the performance of these devices is still hindered by quantum limit and contact resistance. Li et al. [51] reported a significant breakthrough in reducing contact resistance close to the quantum limit by forming strong van der Waals interactions between semi-metallic Sb(0112) and monolayer MoS_2, as well as hybridization of M–S energy bands at the Fermi level. This method realizes an ultralow contact resistance of 42 Ohm micrometres, an on-state current of 1.23 mA per micrometer, and an on/off ratio over 10^8. These performance surpasses equivalent silicon-based semiconductor technologies and meets the 2028 roadmap target. Another feasible stratagem to overcome the Fermi level pinning of 2D semiconductors is edge metal contact, namely, 1D metal contact [17,52]. Using Pd or Au with high work function, high-quality p-type dominant MoS_2 FETs display that the hole mobility is 330 and 432 $cm^2\ V^{-1}\ s^{-1}$ at 300 K, respectively (Fig. 5e) [17]. Fermi level pinning in multilayer MoS_2 is highly dependent on the depletion width and carrier density significantly [52]. Due to the inhomogeneous charge distribution in the vertical direction of multilayer MoS_2, the Fermi level pinning generated in the middle layer can be ignored, while the Fermi level pinning generated in the top and bottom layer can be achieved through 1D edge Au contact. Electrons are injected into the upmost layer of multilayer MoS_2, while holes are injected into the inner layer (Fig. 5f) [52].

3.3. Surface modification

The interface state in metal–semiconductor contact is challenging to avoid. Surface modification of semiconductors can potentially alter the interface structure and interface dipole. For instance, organic molecules can tune the electron affinity of semiconductors [53]. The electron affinity of GaAs(100) increases when decorated with negative molecular dipoles, and decreases when coated with positive molecular dipoles [54]. However, the residual energy of sputtered metal atoms will damage the surface molecular layer, leading to the unstable of SBH [55,56]. Inorganic insulating materials with wide-gap semiconductors, such as BN [37,57], HfO_2 [58], SiO_2 [59], Ta_2O_5 [38], TiO_2 [60], AlO_x [61,62], Ge_3N_4 [63,64], Si_3N_4 [4], MgO [65], and TaN [66], can reduce damage during preparation of metal electrodes due to their high hardness. These thin insulator materials in the metal-insulator-semiconductor (MIS) structure function as the "Fermi level depinning layer", improving the interface behavior parameter. Consequently, the SBH has a strong correlation with the work function of metal [63]. Aside from acting as the insulator in the MIS structure, the dipoles and trap sites on the surface of insulator can function as dopants [27,67], and the Fermi level can be tuned [68,69]. Electron doping from the insulator substrate can minimize the Schottky barrier when SiO_2 and h-BN are used as substrate (Fig. 6a) [69].

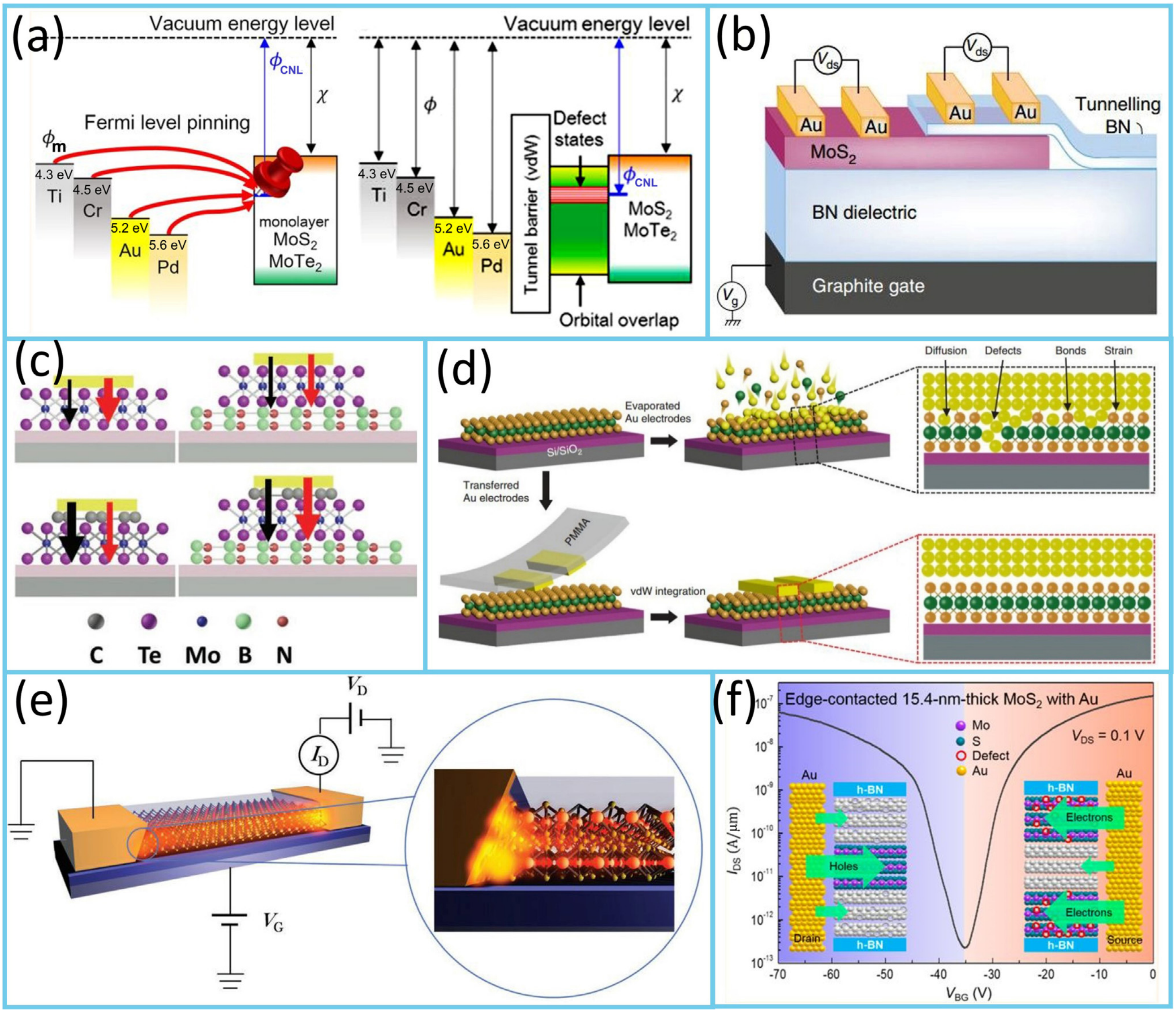

Fig. 5. (Color online) Fermi level pinning and pathways to overcome the Fermi level pinning effect. (a) Fermi level pinning at contact interface of metal and $MoS_2/MoTe_2$. The interface state between metal and $MoS_2/MoTe_2$, including tunnel barrier, orbital overlap and defect states. Reproduced with permission from Ref. [35]. Copyright © 2017 American Chemical Society. (b) Schematics of cross section of Au-MoS_2 contact directly and Au-BN-MoS_2 contact. Reproduced with permission from Ref. [37]. Copyright © 2017, Springer Nature. (c) The diagrams of carrier injection for $MoTe_2$ FETs before and after inserting graphene and BN. Reproduced with permission from Ref. [40]. Copyright © 2018, Wiley-VCH. (d) Fabrication processes of WSe_2 transistors using transferred metal and deposited metal. Reproduced with permission from Ref. [42]. Copyright © 2017, Springer Nature. (e) Schematic diagram of the 1D edge metal contacted FETs. Reproduced with permission from Ref. [17]. Copyright © 2019, Wiley-VCH. (f) Schematics of carrier injection at the edge of Au-MoS_2 contact. Reproduced with permission from Ref. [52]. Copyright © 2019, American Chemical Society.

The insertion of *h*-BN between MoS_2 and SiO_2 generates a significant "dipole alignment effect". This effect is characterized by the interaction between the positive fixed charges of SiO_2 and the negative image charges in the contact metal, leading to a reduction in the work function of the contact metal and a lower effective SBH.

Additionally, the stoichiometric ratio of the insulator also influences the interface state and SBH. For example, interfacial-oxygen-vacancies in the sub-stoichiometric high-κ oxide render them n-type charge transfer dopants [60,70]. The presence of oxygen vacancies and uncompensated Ti atoms in sub-stoichiometric TiO_x ($x < 2$) creates donor states or bands near the conduction band edge of MoS_2 (Fig. 6b) [60], which is the mechanism of the n-type charge transfer dopant. The effective Schottky barrier is significantly lowered by exploiting the doping effect of the sub-stoichiometric TiO_x ($x < 2$). However, *ab initio* density functional theory (DFT) verifies that the doping effect disappears when the purely stoichiometric high-κ oxides act as substrate [60,71,72]. In addition to the doping effect of substrate or top-gated materials, directly adding extra materials into the 2D materials is another well-proven doping method [73–75]. For instance, potassium (K) as a strong donor of electron can realize the n-type charge transfer doping (Fig. 6c) [73]. From the I_{DS}–V_{GS} characteristics of the device in a vacuum, it can be seen that the electron conduction dramatically rises by several orders of magnitude at the positive gate voltage after doping with K (see the right side of Fig. 6c). Besides n-type charge transfer dopants, surface modification can also provide p-type charge transfer dopants [75]. $AuCl_3$, acting as the effective electron acceptor, is commonly used as a p-type charge transfer dopant of MoS_2 owing to its large positive reduction potential [74,75]. Inserting graphene and doping $AuCl_3$ can provide a high concentration of holes at the interface, leading to a downward shift of Fermi level of MoS_2 and lowering the SBH for holes (Fig. 6d) [75].

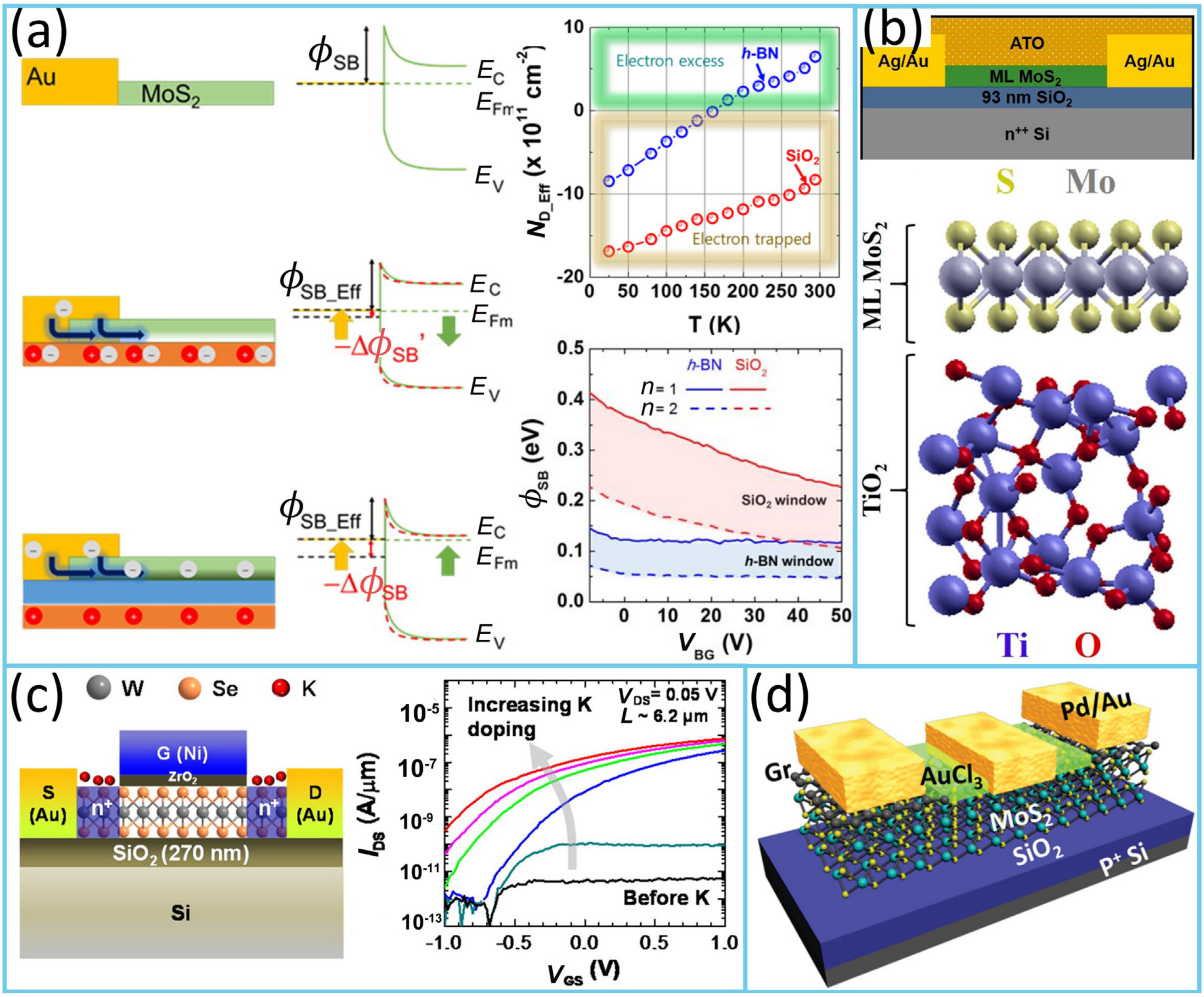

Fig. 6. (Color online) Semiconductor surface modification caused by substrate doping and directly adding extra materials. (a) The surface modification of semiconductor and the corresponding energy-band diagrams with relevant schematics of monolayer MoS_2 on *h*-BN and SiO_2 under considering the substrate doping and dipole alignment. Reproduced with permission from Ref. [69]. Copyright © 2016, American Chemical Society. (b) Crystal structure of ML MoS_2 on the surface of rutile-TiO_2. Reproduced with permission from Ref. [60]. Copyright © 2015, American Chemical Society. (c) Schematic of a top-gated few-layer WSe_2 n-FET by doping K. Transfer characteristics of a 3-layer WSe_2 device (L ~ 6.2 μm) as a function of K exposure time. The black curve is before doping, while the other curves from bottom to top are after 1-, 20-, 40-, 70-, and 120-min doping. Reproduced with permission from Ref. [73]. Copyright © 2013, American Chemical Society. (d) Schematic diagram of a MoS_2 device prepared by doping $AuCl_3$. Reproduced with permission from Ref. [75]. Copyright © 2016, Wiley-VCH.

3.4. Image-lowering effect

Applying an electric field can induce an image-lowering (Schottky) effect, creating an image force that lowers the SBH. This image force stems from the Coulombic attractive force and electric field force induced by the external electric field (Fig. 7a). The $q\phi_m$ (work function of metal) is reduced to $q\phi_B$(effective work function of metal) due to the coupling effect of the Coulombic attractive force and the electric field force (Fig. 7b), leading to the formation of a bare Schottky barrier at the interface of metal and semiconductor. The SBH is significantly lowered at a high external electric field due to the image-lowering effect (Eqs. (3) and (4)) [76]. For metal and n-type semiconductor systems, SBH will slightly increase when a forward bias is applied, while the opposite result can be observed under the reverse bias (Fig. 7c), indicating the SBH is bias dependent [77]. The above theory is based on 3D semiconductors. However, lateral Schottky junctions based on 2D materials offer an opportunity to approach a sharp Schottky barrier without interfacial dipole potential and image-lowering effect [78,79]. Recently, Yao et al. [79] designed the $CrTe_3/CrTe_2$ lateral in-plane Schottky junction with an atomically sharp and seamless interface (Fig. 7d). The sharpness of the Schottky barrier is evidenced by dI/dV spectra of scanning tunneling microscopy across the junction (Fig. 7e), clearly visualizing the profile of energy band bending and SBH of 0.5 eV can be observed. A perfectly triangular-shaped barrier, which is a typical characterization of a Schottky barrier, is shown on the $CrTe_3$ side of the interface (Fig. 7f). This lateral in-plane Schottky junction with the atomically sharp metal-semiconductor interface allows, in principle, a high carrier current along the interface.

The intrinsic barrier height is $q\phi_{Bn0}$. The barrier height at thermal equilibrium is $q\phi_{Bn}$. The lowering amount of Schottky barrier under forward and reverse bias is $q\Delta\phi_F$ and $q\Delta\phi_R$, respectively.

The x_m and $\Delta\phi$ can be given by

$$x_m = \sqrt{\frac{q}{16\pi\varepsilon_s|E_{ex}|}}, \tag{3}$$

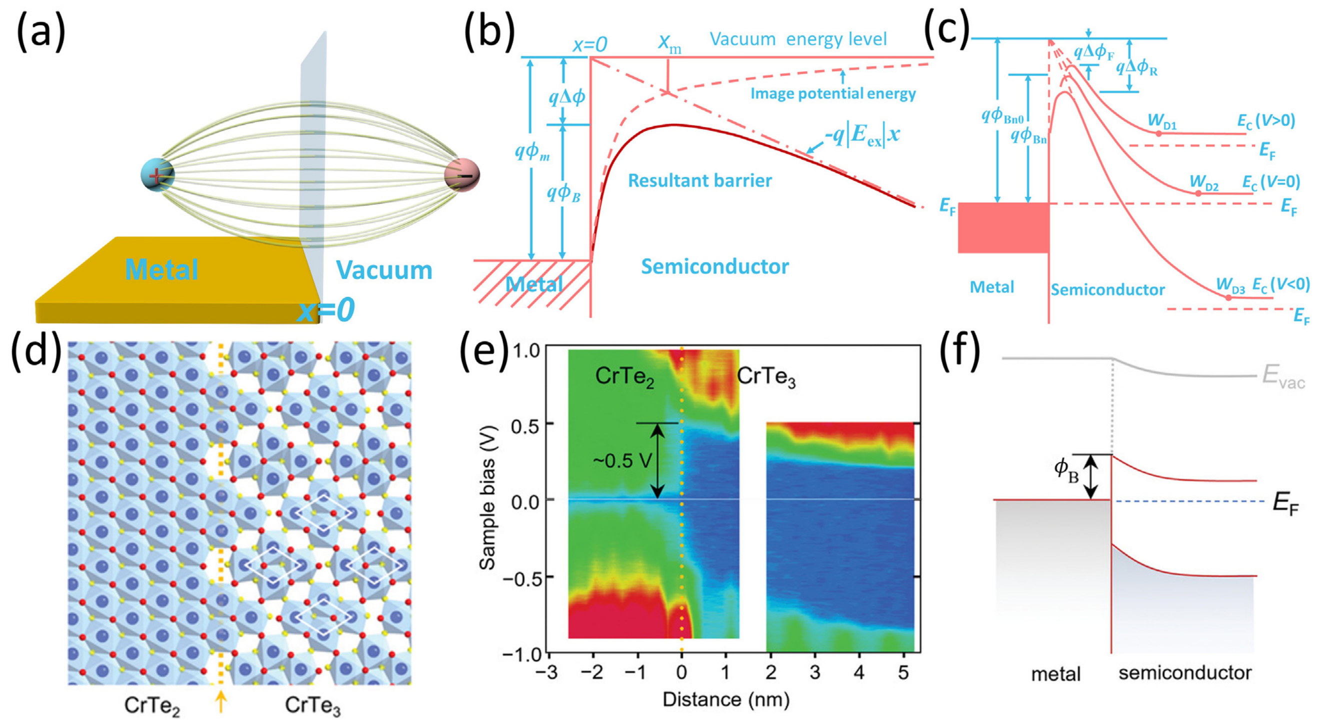

Fig. 7. (Color online) Image lowering effect of Schottky junction. (a) Coulombic attractive force due to the induced image charge. (b) Schottky (or image lowering) effect at the metal-vacuum interface. (c) Under different biasing conditions, the energy-band diagram of metal–semiconductor (n-type) interface after considering Schottky effect. (d) Atomic structural of the $CrTe_2/CrTe_3$ Schottky junction along the direction of the orange arrow. (e) d*I*/d*V* conductance maps around $CrTe_2/CrTe_3$ Schottky junction. (f) A typical schematic band diagram of Schottky junction. Reproduced with permission from Ref. [79]. Copyright © 2022, Wiley-VCH.

$$\Delta\phi = \sqrt{\frac{q|E_{\mathrm{ex}}|}{4\pi\varepsilon}}, \tag{4}$$

where ε_s is the permittivity of semiconductor, and E_{ex} is external electric field.

3.5. External electric field

The SBH can be modulated by the tuning location of the Fermi level. In the case of the n-type semiconductor Schottky junction, a positive gate-voltage applied around the Schottky junction will lower the SBH, while a negative gate-voltage will raise the SBH [80,81]. The opposite phenomenon is observed for the Schottky junction formed by the p-type semiconductor.

In addition, the external voltage can also interact with the point defect in semiconductors. The native point defects inevitably generated during the preparation of semiconductors can form a localized field due to the deficiency of the bonding atom. When an external voltage is applied to the oxide semiconductor, an interaction occurs between the localized field and the generated electrical field. The ionized oxygen vacancies (V_O^+ or V_O^{2+}) are generated by trapping the hole in the localized field around the point defect or exciting the unbound electron by an external electric field ($V_O^0 \rightarrow e + V_O^+$, $V_O^+ \rightarrow e + V_O^{2+}$) [82,83]. These ionized oxygen vacancies can migrate owing to the electric force, and some direct proofs of this phenomenon are found by transmission electron microscopy [84,85], scanning transmission synchrotron X-ray microscopy [86], and electron energy-loss spectroscopy [87]. For Schottky device, the accumulation of ionized oxygen vacancies at the junction interface is equivalent to applying a positive gate-voltage to semiconductors, lowering the SBH for n-type ZnO nanowire devices and raising the SBH for p-type CuO nanowire devices [88–90]. This phenomenon is more pronounced under high electric field intensity. The high pulse voltage and low current properties of the triboelectric nanogenerator (TENG) make it a safe and portable high voltage power source. Meng et al. [88,89] systematically investigated the SBH regulation of ZnO nanowire devices under the high pulse voltage of TENG. They proposed a polarization model for the changes in SBH after being impacted by the TENG voltage (Fig. 8) [88]. The diffusion of ionized oxygen vacancies driven by the electrical force generated by TENG causes them to aggregate at the junction around the interface, lowering the SBH from ϕ_{Bn0} to ϕ_{Bn}.

3.6. Light illumination

If the photon energy is high enough ($h\nu \geq E_g$), photoexcitation generates the electron-hole pairs in depletion of the Schottky junction on the semiconductor side. These photo-generated electron-hole pairs increase the electron or hole concentration in the conduction or valence band of semiconductors. As a result, the Fermi level shifts upwards for Schottky junctions of n-type semiconductor and downwards for p-type semiconductors devices. The SBH will lower owing to the energy band being bent in the opposite direction by the rapid growth of electrons in the conduction band and holes in the valance band [91–93]. The SBH change of n-type (Fig. 9a and b) and p-type semiconductors (Fig. 9c and d) before and after light illumination are depicted in Fig. 9. The reduction of SBH can enhance carrier injection and transport at the metal–semiconductor interfaces. This phenomenon is widely utilized in photoelectron devices based on Schottky contacts.

3.7. Piezotronic effect

The piezotronic effect, which is a field established in 2007 [94], tunes SBH and the carrier transport by piezopotential once a stress is applied to a piezoelectric semiconductor [95–98]. In a Schottky contact based on metal and piezoelectric semiconductors, the

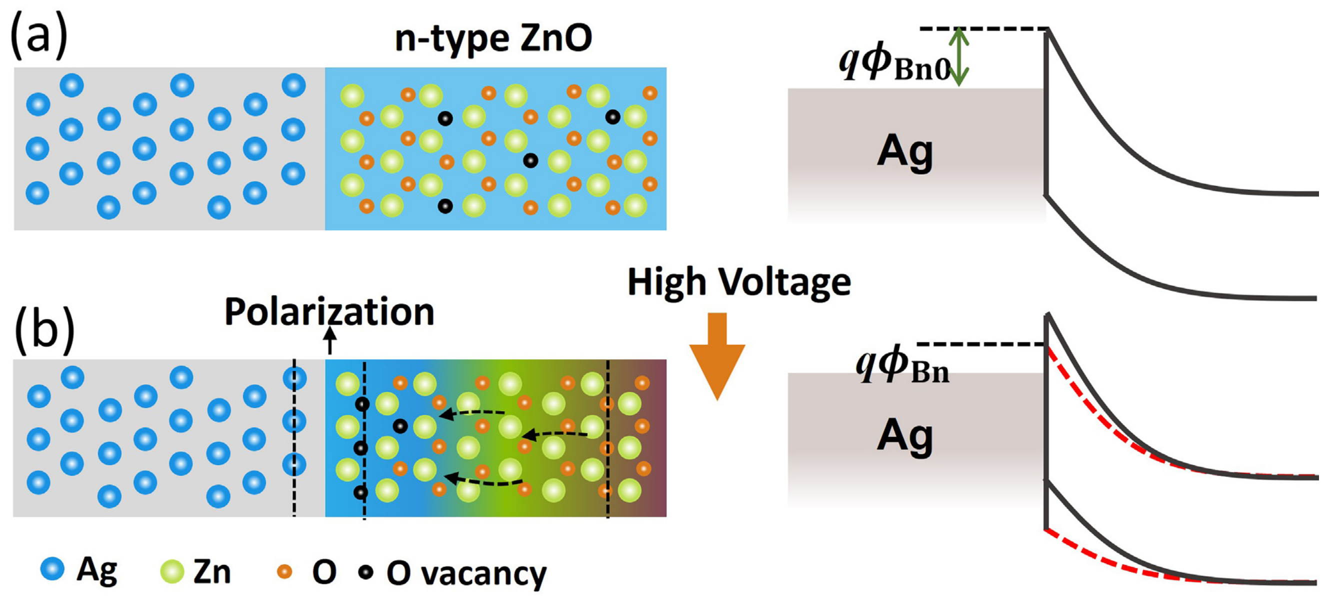

Fig. 8. (Color online) Schematic diagram of polarization model and energy-band diagrams about the variation of SBH after impacting by TENG. (a) Schematic diagram of the atomic structure of Ag-ZnO interface and band diagram of the corresponding Schottky junction. (b) Schematic diagram of oxygen vacancies diffusion and the change of SBH after impacting by high pulse voltage of TENG. Reproduced with permission from Ref. [88]. Copyright © 2020, American Chemical Society.

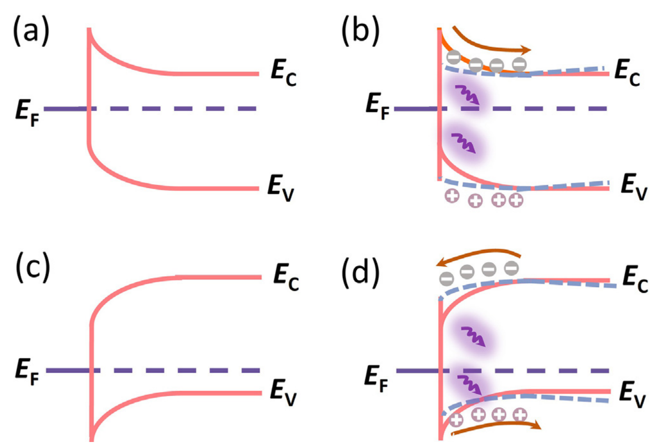

Fig. 9. (Color online) Change of SBH under the light illumination. (a), (b) The change of energy band for Schottky junction based on n-type semiconductor before and after light illumination. (c), (d) The change of energy band for Schottky junction based on p-type semiconductor before and after light illumination. The dashed line in (b) and (d) is the position of conduction band and valence band under light illumination, respectively.

application of stress to the semiconductor results in static polarization charges that cannot be screened. It can modulate the SBH and regulate the carrier transport at the Schottky junction (Fig. 10a and b). The piezoelectric polarization charges act as a "gate voltage" to tune the performance of the Schottky device, such as gas sensors, biosensors, chemical sensors, photodetectors, and strain sensors [99,100]. This highlights the potential of the piezotronic effect in improving the functionality and sensitivity of various sensor devices.

According to Schottky diffusion theory, when a strain is applied to a Schottky junction of metal and piezo-semiconductor, the built-in potential ψ_{bi} can be expressed as

$$\psi_{bi} = \frac{q}{2\varepsilon_s}\left(\rho_{piezo}W_{piezo}^2 + N_D W_{Dn}^2\right) \tag{5}$$

where q represents the element charge, ε_s is the permittivity of ZnO, ρ_{piezo} is the polarization charges density, W_{piezo} is the width of polarization charges, N_D is the donor concentration, and W_{Dn} is the width of depletion region in n-type semiconductor.

The current density across the Schottky junction after piezoelectric polarization can be determined by [101–103]

$$J = J_0 \exp\left(\frac{q^2\rho_{piezo}W_{piezo}^2}{2\varepsilon_s k_B T}\right)\left[\exp\left(\frac{qV}{kT}\right) - 1\right], \tag{6}$$

where V is the bias voltage, k_B and T are the Boltzmann constant and temperature, respectively, J_0 is the saturation current density, and ε_s is the permittivity of semiconductor.

In the case of Schottky junction, J_0 is given by

$$J_0 = \frac{q^2 D_n N_c}{k_B T}\sqrt{\frac{2qN_D(\varphi_{bi0} - V)}{\varepsilon_s}}\exp\left(-\frac{q\phi_{Bn0}}{k_B T}\right), \tag{7}$$

where N_c and D_n are the effective density of states at conduction band and electron diffusion coefficients, respectively, ϕ_{Bn0} and φ_{bi0} are SBH and built-in potential with the absence of polarization charges.

When a stress is applied on the Schottky junction, the SBH can be rewritten as

$$\phi_{Bn} = \phi_{Bn0} - \frac{q\rho_{piezo}W_{piezo}^2}{2\varepsilon_s}. \tag{8}$$

4. Conclusion and perspectives

Adjusting the SBH is crucial for optimizing the performance of metal–semiconductor device. This review presents the formation theory of the Schottky barrier predicted by the Schottky-Mott rule. We then overview static and dynamic approaches for SBH adjustment. Static approaches include metal and interface gap. Dynamic adjustment techniques for the SBH include surface modification, image-lowering effect, external electric field, light illumination, and the piezotronic effect. The mechanisms or theories corresponding to these methods have also been discussed.

While the adjustment methods summarized in this review cover the primary effective techniques, there are still many challenges in further practical applications. More efforts and new

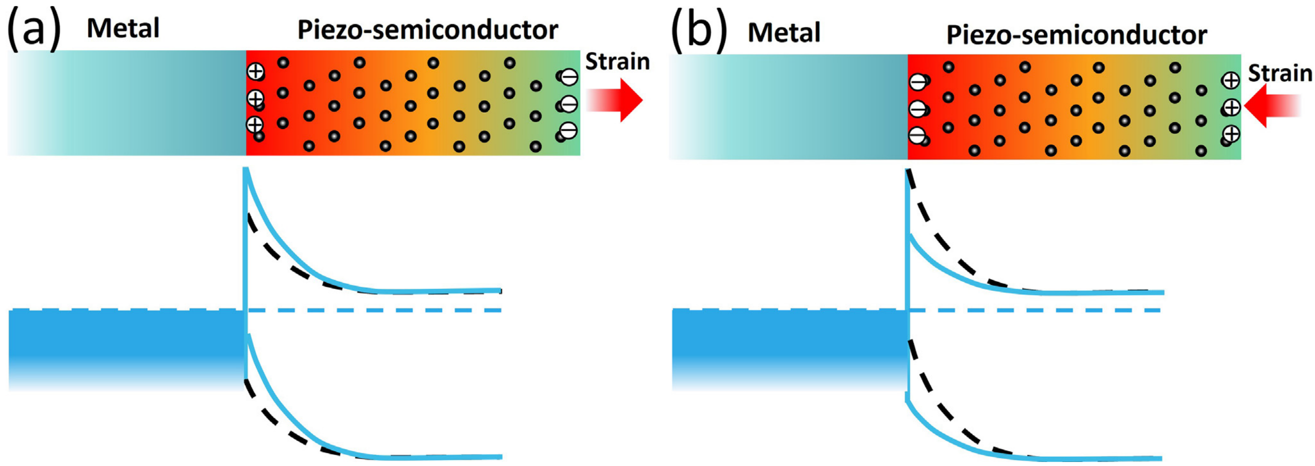

Fig. 10. (Color online) Schematic of energy-band diagram illustrating the piezotronic effect under the tensile strain (a) and compressive strain (b).

technologies need to be introduced into further research to address the challenges, such as the precise measurement of SBH, Fermi level pinning, stability of adjustment methods, transparent metal-like electrode, and low-resistance Ohmic contact.

The continuous progress of measurement technology, and more precise and efficient methods for measuring the SBH are expected. Currently, the value of SBH is indirectly obtained by the calculation from the *I-V* curve. Direct measurement methods, such as scanning tunneling microscopy, conductive atomic force microscopy, can give an accurate value of SBH and help evaluate adjustment methods of SBH. Furthermore, the computational materials science, such as DFT calculations, could assist in predicting the charge density, degree of hybridization and charge transfer at the interface. In addition, the integration of machine learning and computational materials science could potentially accelerate the discovery and optimization of new methods for Schottky barrier modulation.

The inevitable Fermi level pinning induced by the interface gap states makes it difficult to eliminate Schottky barriers. An effective method to eliminate Fermi level pinning is to form van der Waals contact in 2D material-based devices, whereas the existence of a gap introduces a non-negligible tunnel barrier, leading to the high contact resistance and the low efficiency of charge injection. Aim to overcome the tunnel barrier, methods including edge contacts, semi-metal contact, ultrahigh vacuum evaporation, low-energy metal integration, hybridization of M–S energy bands at Fermi energy, have been developed. While these methods can reduce or eliminate the tunnel barrier, their limited industrial compatibility restricts their widespread application. Therefore, further effort is still needed to develop industry-compatible technologies that meet the evolving needs of the semiconductor industry.

Another consideration is the stability of Schottky barrier modulation in dynamic methods. The device performance will be compromised owing to the irreversible change in interface state during the adjustment of SBH.

A transparent metal-like electrode plays a pivotal role in the application of a photodetector or solar cell. Although materials such as graphene, indium tin oxide, fluorine-doped tin oxide, and aluminum-doped zinc oxide are potential candidates as transparent electrodes, there are relatively few options for suitable transparent conductive electrodes to form the appropriate SBH or low resistance Ohmic contact considering the rapid progress of photodetectors and solar cells [104]. Future investigations should focus on transparent metal-like electrodes with tunable work functions and low resistance.

Achieving Ohmic contact or a zero Schottky barrier is vital for the semiconductor industry. However, the interface defects introduce the inevitable Fermi level pinning and Schottky barrier, reducing the efficiency of charge injection. Effort is still needed to pave the way for achieving low resistance Ohmic contacts in next-generation semiconductor of transition-metal dichalcogenides.

Conflict of interest

The authors declare that they have no conflict of interest.

Acknowledgments

This work was supported by Youth Innovation Promotion Association CAS (2023175), the National Natural Science Foundation of China (T2125003), and the Fundamental Research Funds for the Central Universities.

Author contributions

Jianping Meng conceptualized the review. Jianping Meng prepared and revised the manuscript. Jianping Meng, Chengkuo Lee, and Zhou Li discussed the reviewed.

References

[1] Meng J, Li Q, Huang J, et al. Self-powered photodetector for ultralow power density UV sensing. Nano Today 2022;43:101399.
[2] Louie SG, Cohen ML. Electronic-structure of a metal-semiconductor interface. Phys Rev B 1976;13:2461–9.
[3] Nishimura T, Kita K, Toriumi A. Evidence for strong Fermi-level pinning due to metal-induced gap states at metal/germanium interface. Appl Phys Lett 2007;91:123123.
[4] Kobayashi M, Kinoshita A, Saraswat K, et al. Fermi level depinning in metal/Ge Schottky junction for metal source/drain Ge metal-oxide-semiconductor field-effect-transistor application. J Appl Phys 2009;105:023702.
[5] Sotthewes K, van Bremen R, Dollekamp E, et al. Universal Fermi-level pinning in transition-metal dichalcogenides. J Phys Chem C 2019;123:5411–20.
[6] Tung RT. Recent advances in Schottky barrier concepts. Mat Sci Eng R 2001;35:1–138.
[7] Yu RM, Niu SM, Pan CF, et al. Piezotronic effect enhanced performance of schottky-contacted optical, gas, chemical and biological nanosensors. Nano Energy 2015;14:312–39.
[8] Pan CF, Zhai JY, Wang ZL. Piezotronics and piezo-phototronics of third generation semiconductor nanowires. Chem Rev 2019;119:9303–59.
[9] Schottky W. Zur halbleitertheorie der sperrschicht- und spitzengleichrichter. Z Phys 1939;113:367–414.
[10] Mott NF. The theory of crystal rectifiers. Proc R Soc London Ser A 1939;171:27–38.
[11] Tung RT. Chemical bonding and fermi level pinning at metal-semiconductor interfaces. Phys Rev Lett 2000;84:6078–81.
[12] Tung RT. Formation of an electric dipole at metal-semiconductor interfaces. Phys Rev B 2001;64:205310.

[13] Meng J, Li Z. Schottky-contacted nanowire sensors. Adv Mater 2020;32:2000130.
[14] Michaelson HB. The work function of the elements and its periodicity. J Appl Phys 1977;48:4729–33.
[15] Pan YY, Wang YY, Wang L, et al. Graphdiyne-metal contacts and graphdiyne transistors. Nanoscale 2015;7:2116–27.
[16] Das S, Chen HY, Penumatcha AV, et al. High performance multilayer MoS_2 transistors with scandium contacts. Nano Lett 2013;13:100–5.
[17] Yang Z, Kim C, Lee KY, et al. A Fermi-level-pinning-free 1D electrical contact at the intrinsic 2D MoS_2-metal junction. Adv Mater 2019;31:1808231.
[18] Javey A, Guo J, Wang Q, et al. Ballistic carbon nanotube field-effect transistors. Nature 2003;424:654–7.
[19] Mann D, Javey A, Kong J, et al. Ballistic transport in metallic nanotubes with reliable Pd ohmic contacts. Nano Lett 2003;3:1541–4.
[20] Xiang L, Xia F, Jin WL, et al. Carbon nanotube dual-material gate devices for flexible configurable multifunctional electronics. Carbon 2020;161:656–64.
[21] Zhang ZY, Liang XL, Wang S, et al. Doping-free fabrication of carbon nanotube based ballistic CMOS devices and circuits. Nano Lett 2007;7:3603–7.
[22] Zhang H, Xiang L, Yang YJ, et al. High-performance carbon nanotube complementary electronics and integrated sensor systems on ultrathin plastic foil. ACS Nano 2018;12:2773–9.
[23] Bardeen J. Surface states and rectification at a metal semi-conductor contact. Phys Rev 1947;71:717–27.
[24] Saidi WA. Influence of strain and metal thickness on metal-MoS_2 contacts. J Chem Phys 2014;141:094707.
[25] Kang JH, Liu W, Sarkar D, et al. Computational study of metal contacts to monolayer transition-metal dichalcogenide semiconductors. Phys Rev X 2014;4:031005.
[26] Hasegawa H, Sawada T. On the electrical-properties of compound semiconductor interfaces in metal-insulator semiconductor structures and the possible origin of interface states. Thin Solid Films 1983;103:119–40.
[27] Tung RT. The physics and chemistry of the schottky barrier height. Appl Phys Rev 2014;1:011304.
[28] Hu W, Sheng Z, Hou X, et al. Ambipolar 2D semiconductors and emerging device applications. Small Methods 2021;5:2000837.
[29] Liu D, Guo Y, Fang L, et al. Sulfur vacancies in monolayer MoS_2 and its electrical contacts. Appl Phys Lett 2013;103:183113.
[30] Liu Y, Guo J, Zhu EB, et al. Approaching the Schottky-Mott limit in van der Waals metal-semiconductor junctions. Nature 2018;557:696–700.
[31] Gong C, Colombo L, Wallace RM, et al. The unusual mechanism of partial Fermi level pinning at metal-MoS_2 interfaces. Nano Lett 2014;14:1714–20.
[32] Farmanbar M, Brocks G. Controlling the Schottky barrier at MoS_2/metal contacts by inserting a BN monolayer. Phys Rev B 2015;91:161304.
[33] Farmanbar M, Brocks G. First-principles study of van der Waals interactions and lattice mismatch at MoS_2/metal interfaces. Phys Rev B 2016;93:085304.
[34] Liu YY, Stradins P, Wei SH. Van der Waals metal-semiconductor junction: Weak Fermi level pinning enables effective tuning of Schottky barrier. Sci Adv 2016;2:e1600069.
[35] Kim C, Moon I, Lee D, et al. Fermi level pinning at electrical metal contacts of monolayer molybdenum dichalcogenides. ACS Nano 2017;11:1588–96.
[36] Wang JL, Yao Q, Huang CW, et al. High mobility MoS_2 transistor with low Schottky barrier contact by using atomic thick *h*-BN as a tunneling layer. Adv Mater 2016;28:8302–8.
[37] Li XX, Fan ZQ, Liu PZ, et al. Gate-controlled reversible rectifying behaviour in tunnel contacted atomically-thin MoS_2 transistor. Nat Commun 2017;8:970.
[38] Lee S, Tang A, Aloni S, et al. Statistical study on the Schottky barrier reduction of tunneling contacts to CVD synthesized MoS_2. Nano Lett 2016;16:276–81.
[39] Farmanbar M, Brocks G. Ohmic contacts to 2D semiconductors through van der Waals bonding. Adv Electron Mater 2016;2:1500405.
[40] Wang JJ, Wang F, Wang ZX, et al. Controlling injection barriers for ambipolar 2D semiconductors via quasi-van der Waals contacts. Adv Sci 2019;6:1801841.
[41] Quhe RG, Wang YY, Ye M, et al. Black phosphorus transistors with van der Waals-type electrical contacts. Nanoscale 2017;9:14047–57.
[42] Kong LG, Zhang XD, Tao QY, et al. Doping-free complementary WSe_2 circuit via van der Waals metal integration. Nat Commun 2020;11:1866.
[43] Novoselov KS, Mishchenko A, Carvalho A, et al. 2D materials and van der Waals heterostructures. Science 2016;353:aac9439.
[44] Liu Y, Weiss NO, Duan XD, et al. Van der Waals heterostructures and devices. Nat Rev Mater 2016;1:16042.
[45] Liu W, Kang J H, Cao W, et al. High-performance few-layer-MoS_2 field-effect-transistor with record low contact-resistance. In: Proceedings of the 2013 IEEE International Electron Devices Meeting (IEDM). Washington, DC, 2013; 19.4.1-19.4.4.
[46] Kang JH, Liu W, Banerjee K. High-performance MoS_2 transistors with low-resistance molybdenum contacts. Appl Phys Lett 2014;104:093106.
[47] Wang Y, Kim JC, Wu RJ, et al. van der Waals contacts between three-dimensional metals and two-dimensional semiconductors. Nature 2019;568:70–4.
[48] Wang Y, Kim JC, Li Y, et al. P-type electrical contacts for 2D transition-metal dichalcogenides. Nature 2022;610:61–6.
[49] Kwon G, Choi Y-H, Lee H, et al. Interaction- and defect-free van der Waals contacts between metals and two-dimensional semiconductors. Nat Electron 2022;5:241–7.
[50] Shen P-C, Su C, Lin Y, et al. Ultralow contact resistance between semimetal and monolayer semiconductors. Nature 2021;593:211–7.
[51] Li W, Gong X, Yu Z, et al. Approaching the quantum limit in two-dimensional semiconductor contacts. Nature 2023;613:274–9.
[52] Choi H, Moon BH, Kim JH, et al. Edge contact for carrier injection and transport in MoS_2 field-effect transistors. ACS Nano 2019;13:13169–75.
[53] Campbell IH, Rubin S, Zawodzinski TA, et al. Controlling Schottky energy barriers in organic electronic devices using self-assembled monolayers. Phys Rev B 1996;54:14321–4.
[54] Vilan A, Ghabboun J, Cahen D. Molecule-metal polarization at rectifying GaAs interfaces. J Phys Chem B 2003;107:6360–76.
[55] Herdt GC, Jung DR, Czanderna AW. Weak interactions between deposited metal overlayers and organic functional groups of self-assembled monolayers. Prog Surf Sci 1995;50:103–29.
[56] de Boer B, Frank MM, Chabal YJ, et al. Metallic contact formation for molecular electronics: Interactions between vapor-deposited metals and self-assembled monolayers of conjugated mono- and dithiols. Langmuir 2004;20:1539–42.
[57] Cui X, Shih EM, Jauregui LA, et al. Low-temperature ohmic contact to monolayer MoS_2 by van der Waals bonded Co/*h*-BN electrodes. Nano Lett 2017;17:4781–6.
[58] Chen HI, Chang CH, Lu HH, et al. Hydrogen sensing performance of a Pd/HfO_2/GaN metal-oxide-semiconductor (MOS) Schottky diode. Sens Actuators B 2018;262:852–9.
[59] Tsai TH, Huang JR, Lin KW, et al. Improved hydrogen sensing characteristics of a Pt/SiO_2/GaN Schottky diode. Sens Actuators B 2008;129:292–302.
[60] Rai A, Valsaraj A, Movva HCP, et al. Air stable doping and intrinsic mobility enhancement in monolayer molybdenum disulfide by amorphous titanium suboxide encapsulation. Nano Lett 2015;15:4329–36.
[61] Zhou Y, Ogawa M, Han XH, et al. Alleviation of Fermi-level pinning effect on metal/germanium interface by insertion of an ultrathin aluminum oxide. Appl Phys Lett 2008;93:202105.
[62] Nishimura T, Kita K, Toriumi A. A significant shift of Schottky barrier heights at strongly pinned metal/germanium interface by inserting an ultra-thin insulating film. Appl Phys Express 2008;1:051406.
[63] Lieten RR, Afanas'ev VV, Thoan NH, et al. Mechanisms of Schottky barrier control on n-type germanium using Ge_3N_4 interlayers. J Electrochem Soc 2011;158:G358–62.
[64] Lieten RR, Degroote S, Kuijk M, et al. Ohmic contact formation on n-type Ge. Appl Phys Lett 2008;92:022106.
[65] Zhou Y, Han W, Wang Y, et al. Investigating the origin of Fermi level pinning in Ge Schottky junctions using epitaxially grown ultrathin MgO films. Appl Phys Lett 2010;96:102103.
[66] Wu Z, Huang W, Li C, et al. Modulation of Schottky barrier height of metal/TaN/n-Ge junctions by varying TaN thickness. IEEE Trans Electron Devices 2012;59:1328–31.
[67] Rai A, Movva HCP, Roy A, et al. Progress in contact, doping and mobility engineering of MoS_2: An atomically thin 2D semiconductor. Crystals 2018;8:316.
[68] Park HY, Lim MH, Jeon J, et al. Wide-range controllable n-doping of molybdenum disulfide (MoS_2) through thermal and optical activation. ACS Nano 2015;9:2368–76.
[69] Joo MK, Moon BH, Ji H, et al. Electron excess doping and effective Schottky barrier reduction on the MoS_2/*h*-BN hetero-structure. Nano Lett 2016;16:6383–9.
[70] Alharbi A, Shahrjerdi D. Contact engineering of monolayer CVD MoS_2 transistors. In: Proceedings of the 2017 75th Annual Device Research Conference. South Bend, 2017; 1-2.
[71] Valsaraj A, Chang JW, Rai A, et al. Theoretical and experimental investigation of vacancy-based doping of monolayer MoS_2 on oxide. 2D Mater 2015;2:045009.
[72] McClellan CJ, Yalon E, Smithe KKH, et al. Effective n-type doping of monolayer MoS_2 by AlO_x. In: Proceedings of the 2017 75th Annual Device Research Conference. South Bend, 2017.
[73] Fang H, Tosun M, Seol G, et al. Degenerate n-doping of few-layer transition metal dichalcogenides by potassium. Nano Lett 2013;13:1991–5.
[74] Choi MS, Qu D, Lee D, et al. Lateral mos_2 p-n junction formed by chemical doping for use in high-performance optoelectronics. ACS Nano 2014;8:9332–40.
[75] Liu XC, Qu DS, Ryu JJ, et al. P-type polar transition of chemically doped multilayer MoS_2 transistor. Adv Mater 2016;28:2345–51.
[76] Sze K K N S M. Physics-of-Semiconductor-Devices. New York: John Wiley & Sons, Inc. ; 1981.
[77] Nam CY, Tham D, Fischer JE. Disorder effects in focused-Ion-beam-deposited Pt contacts on GaN nanowires. Nano Lett 2005;5:2029–33.
[78] Zhang JF, Xie WY, Zhao JJ, et al. Band alignment of two-dimensional lateral heterostructures. 2D Mater 2017;4:015038.
[79] Yao J, Wang H, Yuan BK, et al. Ultrathin van der waals antiferromagnet $CrTe_3$ for fabrication of in-plane $CrTe_3$/$CrTe_2$ monolayer magnetic heterostructures. Adv Mater 2022;34:2200236.
[80] Fan ZY, Lu JG. Electrical properties of ZnO nanowire-field effect transistors characterized with scanning probes. Appl Phys Lett 2005;86:032111.
[81] Pan C, Yu R, Niu S, et al. Piezotronic effect on the sensitivity and signal level of Schottky contacted proactive micro/nanowire nanosensors. ACS Nano 2013;7:1803–10.
[82] Lany S, Zunger A. Anion vacancies as a source of persistent photoconductivity in ii–vi and chalcopyrite semiconductors. Phys Rev B 2005;72:035215.

[83] Huang BL, Sun MZ, Peng DF. Intrinsic energy conversions for photon-generation in piezo-phototronic materials: A case study on alkaline niobates. Nano Energy 2018;47:150–71.
[84] Ding Y, Liu Y, Niu SM, et al. Pyroelectric-field driven defects diffusion along *c*-axis in ZnO nanobelts under high-energy electron beam irradiation. J Appl Phys 2014;116:154304.
[85] Kwon D-H, Kim KM, Jang JH, et al. Atomic structure of conducting nanofilaments in TiO_2 resistive switching memory. Nat Nanotechnol 2010;5:148–53.
[86] Kumar S, Wang Z, Huang X, et al. Conduction channel formation and dissolution due to oxygen thermophoresis/diffusion in hafnium oxide memristors. ACS Nano 2016;10:11205–10.
[87] Cooper D, Baeumer C, Bernier N, et al. Anomalous resistance hysteresis in oxide reram: Oxygen evolution and reincorporation revealed by *in situ* TEM. Adv Mater 2017;29:1700212.
[88] Meng JP, Li H, Zhao LM, et al. Triboelectric nanogenerator enhanced Schottky nanowire sensor for highly sensitive ethanol detection. Nano Lett 2020;20:4968–74.
[89] Zhao LM, Li H, Meng JP, et al. Reversible conversion between Schottky and Ohmic contacts for highly sensitive, multifunctional biosensors. Adv Funct Mater 2020;30:1907999.
[90] Meng J, Li Q, Huang J, et al. Tunable schottky barrier height of a Pt–CuO junction via a triboelectric nanogenerator. Nanoscale 2021;13:17101–5.
[91] Hu Y, Chang Y, Fei P, et al. Designing the electric transport characteristics of ZnO micro/nanowire devices by coupling piezoelectric and photoexcitation effects. ACS Nano 2010;4:1234–40.
[92] Li C, Bando Y, Liao MY, et al. Visible-blind deep-ultraviolet Schottky photodetector with a photocurrent gain based on individual Zn_2GeO_4 nanowire. Appl Phys Lett 2010;97:161102.
[93] Yang Q, Guo X, Wang W, et al. Enhancing sensitivity of a single ZnO micro-/nanowire photodetector by piezo-phototronic effect. ACS Nano 2010;4:6285–91.
[94] Wu WZ, Wang ZL. Piezotronics and piezo-phototronics for adaptive electronics and optoelectronics. Nat Rev Mater 2016;1:16031.
[95] Wang ZL. Nanopiezotronics. Adv Mater 2007;19:889–92.
[96] Wang ZL. Piezotronic and piezophototronic effects. J Phys Chem Lett 2010;1:1388–93.
[97] Wang ZL. Piezopotential gated nanowire devices: Piezotronics and piezo-phototronics. Nano Today 2010;5:540–52.
[98] Wang ZL. Progress in piezotronics and piezo-phototronics. Adv Mater 2012;24:4632–46.
[99] Zhou J, Fei P, Gu YD, et al. Piezoelectric-potential-control led polarity-reversible Schottky diodes and switches of ZnO wires. Nano Lett 2008;8:3973–7.
[100] Gao ZY, Zhou J, Gu YD, et al. Effects of piezoelectric potential on the transport characteristics of metal-ZnO nanowire-metal field effect transistor. J Appl Phys 2009;106:113707.
[101] Zhang Y, Liu Y, Wang ZL. Fundamental theory of piezotronics. Adv Mater 2011;23:3004–13.
[102] Wang ZL, Wu W. Piezotronics and piezo-phototronics: Fundamentals and applications. Nat Sc Rev 2014;1:62–90.
[103] Liu Y, Zhang Y, Yang Q, et al. Fundamental theories of piezotronics and piezo-phototronics. Nano Energy 2015;14:257–75.
[104] Li Z, Yan T, Fang X. Low-dimensional wide-bandgap semiconductors for UV photodetectors. Nat Rev Mater 2023;8:587–603.

Jianping Meng is an associate professor at Beijing Institute of Nanoenergy and Nanosystems, and School of Nanoscience and Technology, University of Chinese Academy of Sciences. He received his Ph.D. degree from General Research Institute for Nonferrous Metals, China, in 2017, Master's degree from China University of Geosciences (Beijing), China, in 2013, and Bachelor's degree from Liaoning Technical University, China, in 2010. His research interest focuses on heterojunction device, photodetector, gas sensor and biosensor.

Chengkuo Lee is an associate professor at the Department of Electrical and Computer Engineering of National University of Singapore. He received the Ph.D. degree in Precision Engineering from the University of Tokyo, Tokyo, Japan, in 1996. His research interest focuses on optical MEMS, biomedical MEMS, nanophotonics, and energy harvesters.

Zhou Li is a professor at the Beijing Institute of Nanoenergy and Nanosystems, and School of Nanoscience and Technology, University of Chinese Academy of Sciences. He received his Ph.D. degree from Peking University, China, in 2010, and his bachelor's degree from Wuhan University, China, in 2004. His research interest focuses on bioelectronics, nanogenerators, self-powered medical systems, nano-biosensors, and single cell mechanics.